7.3 Physical and Thermal Mechanical Characterization of Non-Irradiated MAX Phase Materials (Ti-Si-C and Ti-Al-C Systems) — C. Shih, R. Meisner, W. Porter, Y. Katoh, and S. J. Zinkle (Oak Ridge National Laboratory)

OBJECTIVE

The main objective of this work is to investigate the physical and thermal mechanical properties of two commercially available MAX phase materials, nominally Ti_3SiC_2 and Ti_2AlC, at non-irradiated states.

SUMMARY

The physical and thermo mechanical properties of two commercially available MAX phase materials have been characterized in the non-irradiated states including: density, X-ray diffraction analysis, microstructure analysis by SEM, coefficient of thermal expansion, thermal diffusivity, thermal conductivity, dynamic Young's modulus, electrical conductivity, and equibiaxial fracture strength (including Weibull modulus). The results show that the materials contain multiple phases. However, predominate phases are hexagonal MAX phases composed of Ti-SiC-C and Ti-Al-C ternary systems. High thermal and electrical conductivity, adequate Young's modulus and equibiaxial fracture strength were observed. All the properties studied agree well with data from the literature.

PROGRESS AND STATUS

Introduction

MAX phase materials are ternary compounds with the general formula of $M_{n+1}AX_n$ (n = 1, 2, or 3) where M is an early transition metal, A is an A-group element and X is C or N. These materials have hexagonal lattice structures with unique properties that "bring together some of the best attributes of ceramics and metals" [1]. Like ceramics, they are oxidation, creep and fatigue resistant. They show reasonable mechanical properties at high temperatures [2]. On the other hand, they possess metal-like properties, including high electrical and thermal conductivity, excellent machinability, and damage tolerance in certain conditions. Because of their unique properties, the MAX phase materials have seen a lot of research activities in the past few decades. They are considered promising materials for applications where high temperature strength and corrosion resistance are required.

The unique properties of MAX phase materials have also attracted attention from the nuclear research community [3-8]. Proposed nuclear applications include: oxidation barrier coating for the fuel cladding systems in the light water reactors and core components for advanced reactor concepts including the gas fast reactors [4]. Moreover, these ceramics are being studied for fundamental irradiation responses in the US fusion materials program as novel materials that potentially possess radiation tolerance or bring on new scientific insight toward future development of innovative radiation resistant materials. The primary objective of present study is to characterize some of the MAX phase ceramics, which have been subjected to a fundamental neutron irradiation effects study in the High Flux Isotope Reactor, in a non-irradiated condition.

Experimental

Materials

Nominally Ti_3SiC_2 and Ti_2AlC blocks (150 × 44 × 35 mm) were purchased from 3-ONE-2, LLC (Willow Grove, PA). According to the vendor, the materials are fabricated by cold isostatic pressing of pre-reacted ternary carbide powers followed by pressureless sintering. The materials were machined into different shapes for individual characterization method.

Density

The nominally 25 × 2 × 1.5 mm multi-purpose rectangular samples and nominally 6 mm diameter, 1.5 mm thick thermal diffusivity discs were used to determine the density by measuring the mass and bulk volume. The mass of each sample was determined by a Sartorius Genius lab balance to an accuracy of 0.01 mg. The dimensions of the samples were measured by a Mitutoyo micrometer to an accuracy of 1 mm. The volume is calculated using the measured dimensions. The bulk density is simply calculated as the measured mass divided by the bulk volume.

XRD

Continuous q-2q scans were performed on the Panalytical Xpert diffractometer from nominally 10 to 60° 2q in 60 min scans using MoKa radiation (l=0.709319 Å) or CuKa radiation (l=1.540598 Å) and the X'Celerator detector. All scans used ¼° fixed slits and ½° anti-scatter slit. A search match was conducted using the "Jade" and/or High Score software and the ICDD database.

Scanning electron microscopy (SEM)

The samples were mounted in epoxy and polished with a serious of diamond suspension to obtain a mirror finish. Microstructure of the polished samples was examined using either a Hitachi S4700 or a Hitachi S4800 field emission gun SEM.

Coefficient of thermal expansion (CTE)

The samples used for CTE measurement have dimensions of 25 × 2 × 1.5 mm. A NETZSCH DIL 402 CD Thermal Expansion Dilatometer was used to measure the CTE of the samples in vacuum for temperatures from ~25 °C to 1000 °C at a temperature ramp rate of 3 °C per minute.

Thermal diffusivity and thermal conductivity

The samples used for thermal diffusivity, and heat capacity measurements are cylindrical discs with a diameter of 6 mm and a thickness of 1.5 mm. Thermal diffusivity was measured following the guidelines of ASTM E1461 using a NETZSCH LFA 457 Micro Flash Laser Flash Thermal Diffusivity Apparatus. The thermal conductivity is calculated using the measured thermal diffusivity, heat capacity and density according to equation 1

$$k = \alpha \cdot \rho \cdot C_p \tag{1}$$

where k is the thermal conductivity, a the thermal diffusivity, r the density, and C_p the heat capacity. Measurements were done at room temperature and from 100°C to 1000°C with

100°C intervals in flowing ultra-high purity argon gas. The temperature ramp rate was 10°C per minutes or less and a dwell time of 30 minutes were used before each measurement to ensure the equilibrium temperature was reached.

Dynamic Young's modulus

The dynamic Young's modulus (sonic elastic modulus) was measured by the impulse excitation and vibration method following the guidelines of ASTM C1259-08 using a GrindoSonic Mk5 Industrial Non-Destructive Elastic Property Measurement System. The specimen size was 25 × 2 × 1.5 mm. Ten measurements were recorded for each specimen and the average was reported.

Electrical conductivity

The electrical conductivity was measured using the four-point probe method following the guidelines of ASTM C611-98 with a sample dimension of 25 × 2 × 1.5 mm. A probe distance of 10 mm and a cross sample current of 10 mA were used. The current was generated using a KEITHLEY 2400 Source Meter and the voltage drop across the two probes was measured using a KEITHLEY 2192A Nonovoltmeter. Sixteen measurements were conducted on each sample using different geometry combinations. All the measurements were conducted at room temperature.

Equibiaxial fracture strength and Weibull modulus

The room temperature equibiaxial (ring on ring) fracture strength was measured following the guidelines of ASTM C1499-09 with a sample dimension of 6 × 6 × 0.5 mm. This test method is chosen to evaluate the mechanical properties of the materials because of several advantages including: ease of operation, small sample volume compatible, which is important for irradiation studies, and high temperature testing compatible. From our past experience with graphite materials, this test method has shown to generate data with decent quality and statistical distribution. For each material, 30 samples were tested in order to obtain a representative average fracture strength and Weibull modulus.

The Ti_3SiC_2 and Ti_2AlC are expected to have a ductile to brittle transition temperature (DBTT) between 900 to 1200°C. In order to determine this DBTT and any change in DBTT following irradiation, a high temperature equibiaxial fracture fixture has been designed and is now under machining as of December of 2013.

Results and Discussion

Density

Bulk densities of the disc and rectangular bar samples are summarized in Table 1. For both materials, there is no notable difference between samples of the same shape and between two difference sample shapes. The data scattering is very low with coefficient of variation around 0.5%, indicating both good machining quality and material homogeneity. The obtained density agrees well with the reported theoretical density in the open literature [2, 9], but appears to be about 3-4% smaller, suggesting the presence of micro porosity and/or impurity phases in the microstructure.

Table 1. Density, electrical resistivity, Young's modulus, and flexural strength of the non-irradiated materials.

	# of samples	Ti-Si-C	Ti-Al-C
density, disc specimens (g/cm^3)	22	4.390 (0.021)	3.964 (0.035)
density, bar specimens (g/cm^3)	13	4.360 (0.023)	3.923 (0.024)
Electrical resistivity (ohm-m)	13	2.85×10^{-7} (5.39×10^{-9})	4.67×10^{-7} (1.87×10^{-8})
Young's modulus (GPa)	13	313.4 (6.2)	250.8 (6.5)
Flexural strength (MPa)	30	445 (29)	308 (16)

Numbers in the parenthesis represent one standard deviation to the mean

XRD profiles of non-irradiated samples

The XRD profile of the Ti-Si-C sample is presented in Figure 1 where identified peaks are labeled. The software calculated phase composition of this sample is 70.4 wt. % Ti_3SiC_2, 23.8 wt. % TiC, and 5.7 wt. % $TiSi_2$. Very similar XRD calculated phase composition for Ti_3SiC_2 blocks purchased from the same company has been reported by Nappe et al [7]. It is worth mentioning that some of the peaks in the XRD are not identified.

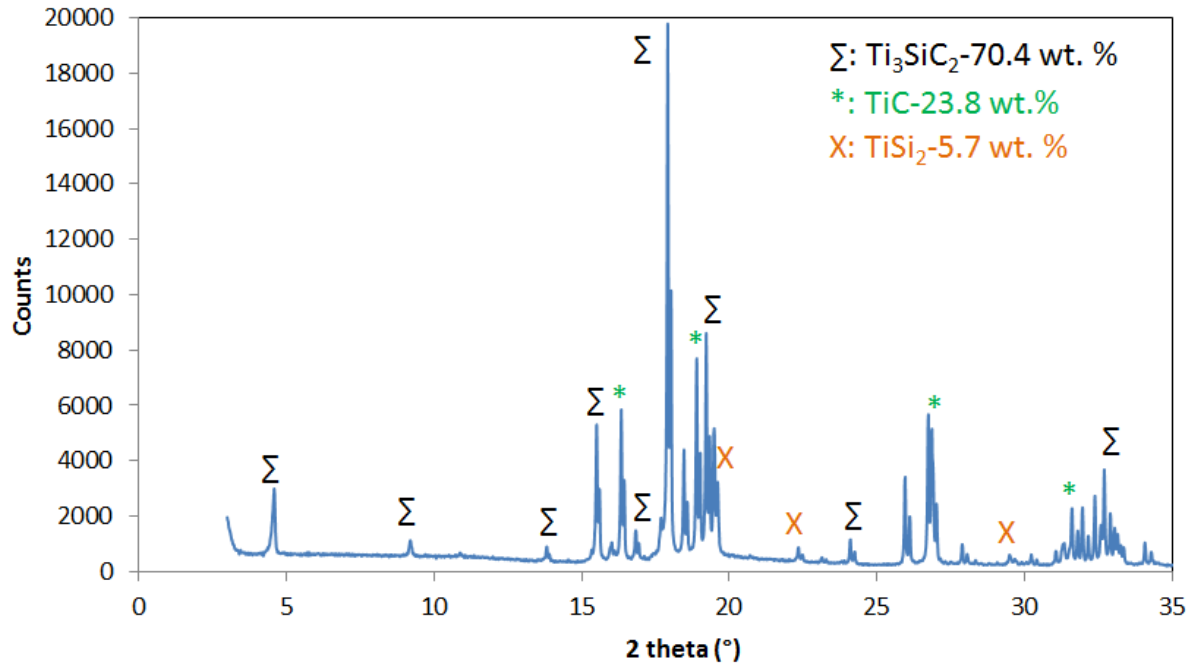

Figure 1. XRD profile of Ti_3SiC_2.

The XRD profile of the Ti-Al-C sample is shown in Figure 2 where identified peaks are labeled. The software calculated phase composition of this sample is 43.3 wt. % Ti_3AlC_2, 16.0 wt. % Ti_2AlC, 34.3 wt. % $Ti_5Al_2C_3$ and 6.4 wt. % $Al_{11}Ti_5$. This results suggest that the nominally Ti_2AlC block actually contains mostly Ti_3AlC_2 and $Ti_5Al_2C_3$ phases. The $Ti_5Al_2C_3$ phase has been synthesized and characterized in bulk only recently [1, 10]. The lattice structure can be described as alternating layers of Ti_2AlC and Ti_3AlC_2. For this reason, the major physical properties of $Ti_5Al_2C_3$, including density, electrical conductivity, thermal conductivity, coefficient of thermal expansion, and elastic properties, are believed and have been reported [1] to be very similar to those of Ti_2AlC and Ti_3AlC_2.

In the paper that characterized the structure of $Ti_5Al_2C_3$ [10], the material is synthesized from heating Ti_2AlC powers (from the same vender as this study) under flowing argon to 1500 °C. The fact that our nominally Ti_2AlC material contains other phases indicates that there might be some processing errors, presumably from heat treatment temperatures, caused further phase transformation from Ti_2AlC to Ti_3AlC_2, $Ti_5Al_2C_3$, and $Al_{11}Ti_5$. It should be noted that predominate phases are all hexagonal MAX phases composed of Ti, Al, and C ternary system.

Since the nominally Ti_3SiC_2 and Ti_2AlC samples contain other phases, hereafter they are referred as Ti-Si-C and Ti-Al-C, respectively, in this report.

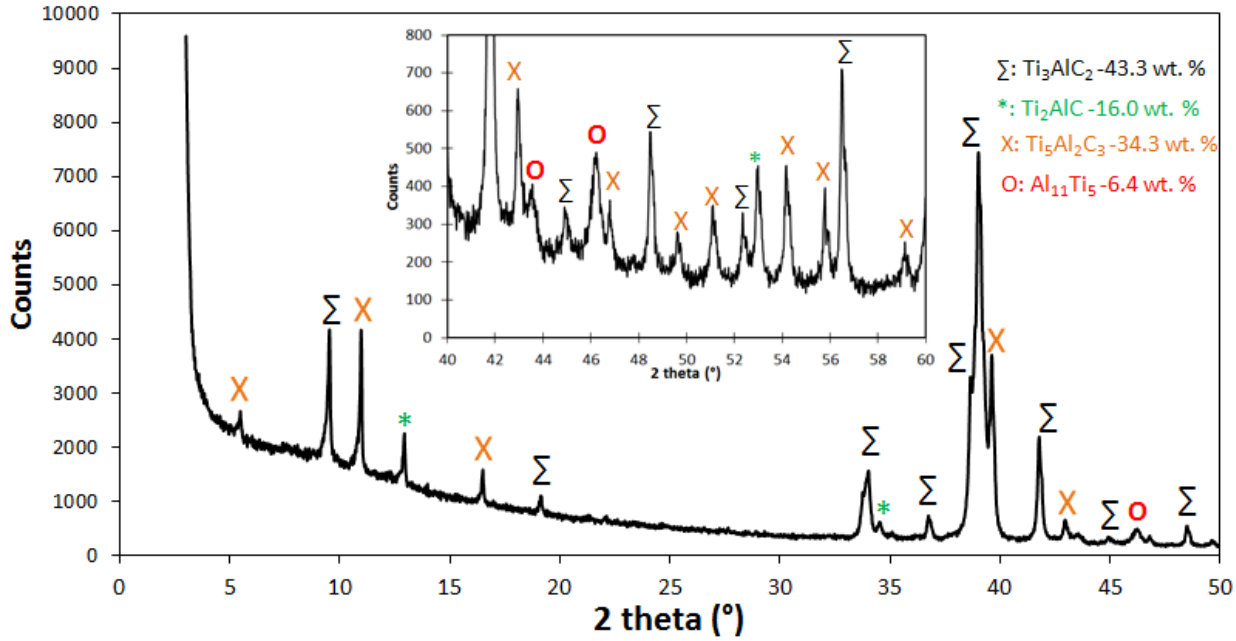

Figure 2. XRD profile of Ti_2AlC.

SEM

Secondary and back-scattered SEM images of the polished Ti-Si-C sample are shown in Figure 3. The very bright areas in the secondary electron images (Figure 3a and c) are identified as pores. The material is not 100% dense and the observed pores correspond to the lowered density as discussed previously. Those pores have a dimension of smaller than 4 mm and are located at grain boundaries. A closer look at the microstructures revealed three distinct contrasts: the elongated grain that appears in bright contrast, the more round shaped dark grain and the island-like grains with ragged boundaries, which are indicated with white arrows in Figure 3d. By cross-referencing the energy dispersive x-ray spectroscopy (EDS) element composition results and the XRD phase composition results, the elongated bright grains are identified as Ti_3SiC_2, the round dark grain are identified as TiC, and the ragged island grains are identified as $TiSi_2$. The percent weight composition observed by the SEM images corresponds well with that calculated from the XRD profiles.

SEM images of the polished Ti-Al-C sample are shown in Figure 4. The areas with very bright edges in Figure 4a are identified as pores. Ti-Al-C sample appears to have slightly less porosity than Ti-Si-C. Three phases are identified and labeled in Figure 4d as bright grains, dark grains and background matrix. Both bright and dark grains showed elongated shapes with width in the range of 4 to 10 mm and length of over 50 mm. The aspect ratio of the grains in Ti-Al-C sample appears to be larger than those seen in Ti-Si-C sample.

In the back-scattered electron (BSE) image in Figure 4d, the brightness differences between different elongated grains are minor, suggesting similar average atomic weight. However, the matrix appears to be significantly darker, suggesting a much-lowered average atomic weight. Cross-referencing between the BSE images, the EDS element composition results and the XRD phase composition results suggest that the elongated grains are Ti_2AlC, Ti_3AlC_2, and $Ti_5Al_2C_3$.

Since all three MAX phase compounds have similar average atomic weight and similar theoretical density, the brightness difference of those phases from the BSE image is expected to be minor. If we further consider that the crystal orientation of each grain affects its brightness, we can conclude that it is difficult to unambiguously assign a phase to each grain unless rigorous EDS analysis is conducted. The dark matrix is likely the $Al_{11}Ti_5$ phase, which has a tetragonal structure with space group I4/mmm. Even though $Al_{11}Ti_5$ also has a similar average atomic weight to the other MAX phases in the sample, is has a significantly lower theoretical density of 3.5 g/cm^3 while the three MAX phases all have a theoretical density of ~4.2 g/cm^3. This lower density explains the lower brightness of $Al_{11}Ti_5$ grains in the BSE image.

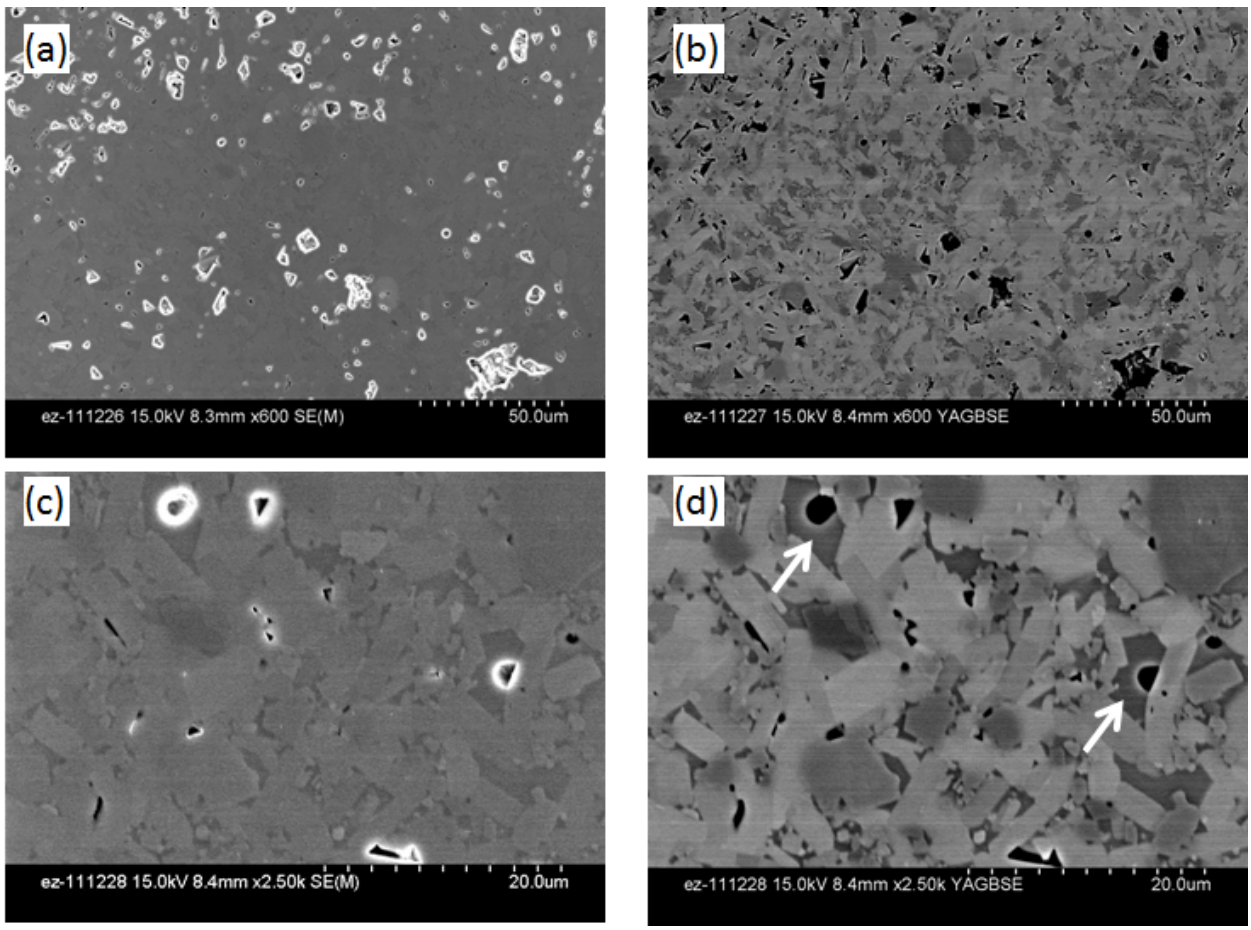

Figure 3. SEM images of (nominally) Ti_3SiC_2 sample. (a) and (c): secondary electron images; (b) and (d): back scattered electron images.

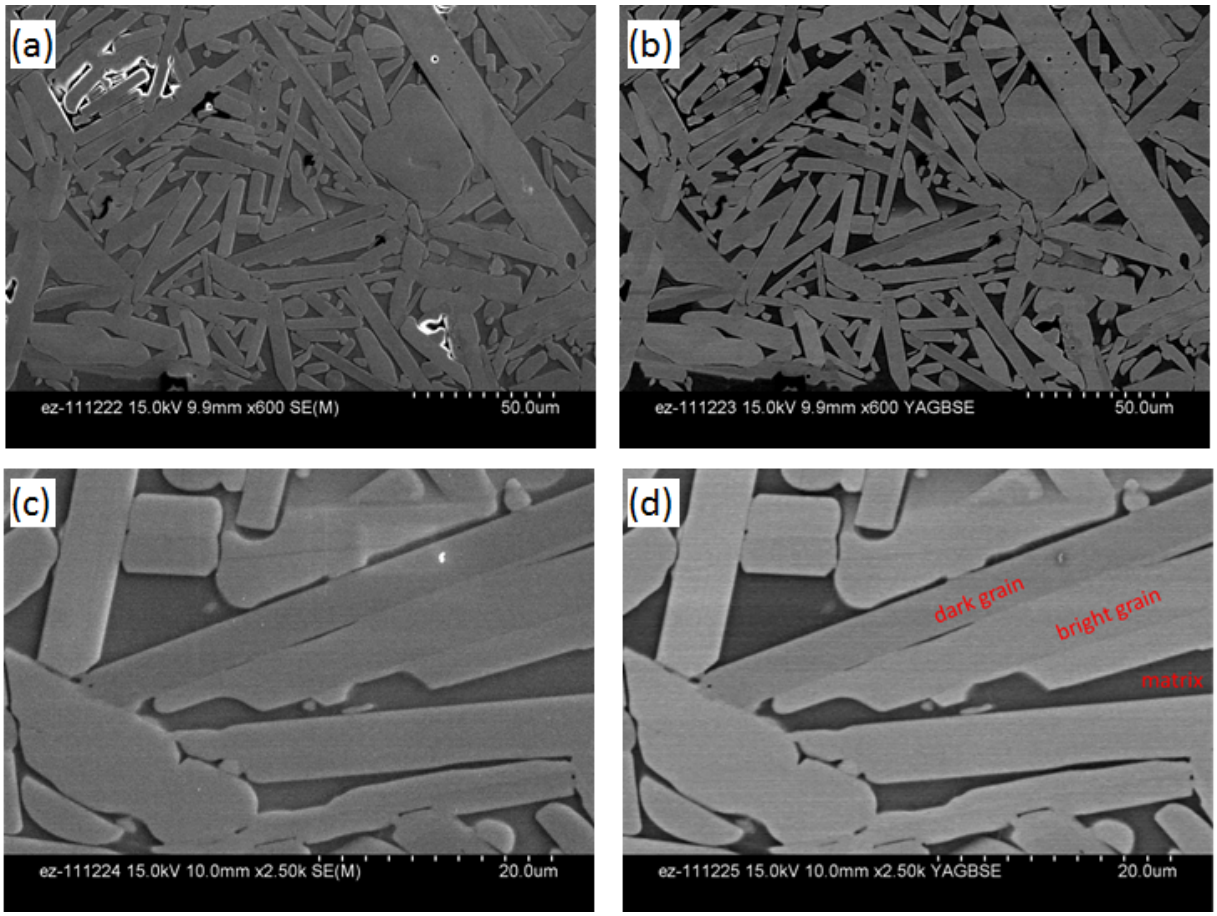

Figure 4. SEM images of (nominally) Ti_2AlC sample. (a) and (c): secondary electron images; (b) and (d): back scattered electron images.

Coefficient of thermal expansion (CTE)

The CTE of Ti-Si-C and Ti-Al-C is shown in Figure 5. Ti-Si-C has a CTE of ~7-9 × 10^{-6} K^{-1}, while Ti-Al-C showed a CTE of 8-10 × 10^{-6} K^{-1}. CTE of both materials increases with increasing temperature. If we use beta CVD SiC as a reference material, which has a CTE of ~4.5 × 10^{-6} per °C at this temperature range, the MAX phase materials in this study showed higher CTE values. They also showed higher CTE values than Zircaloy-4 cladding tubes in the circumferential direction (4.4 × 10-6 K^{-1} at room temperature.

The measured CTE of Ti-Si-C is similar to the reported value (10 × 10^{-6} per °C) for hot isotactic pressed Ti_3SiC_2 [9]. Moreover, the measured CTE of Ti-Al-C corresponds well with the reported CTE of Ti_2AlC and Ti_3AlC_2 [11], which is in the range of 8-9 × 10^{-6} per °C.

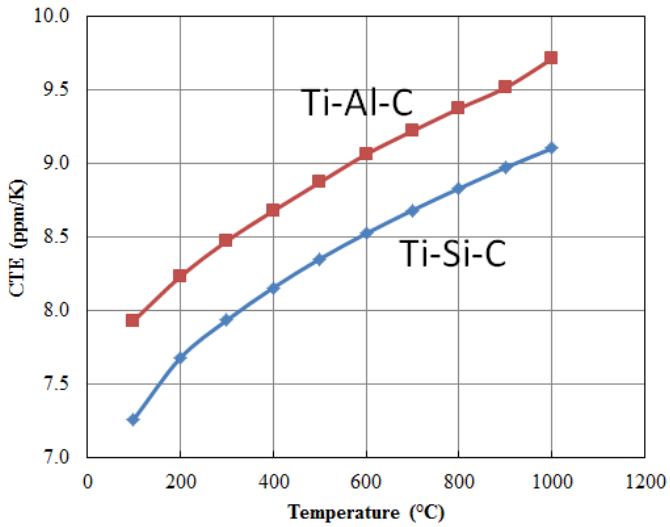

Figure 5. Coefficient of thermal expansion referenced to room temperature for Ti-Si-C and Ti-Al-C.

Thermal diffusivity and thermal conductivity

The heat capacity (C_p) of the two materials is shown in Figure 6 as a function of temperature. Ti-Si-C showed a higher heat capacity than Ti-Al-C at all temperatures. Heat capacity (C_p) of Ti-Si-C in this report is higher than C_p of Ti_3SiC_2 reported in the literature, which is about 0.56 to 0.59 J/g·K [14, 15] at room temperature. Large specimen-to-specimen variation is also observed. TiC is a main impurity in the Ti-Si-C samples. However, its C_p is not particularly higher than Ti_3SiC_2 and thus cannot explain the higher C_p in the Ti-Si-C samples. It's likely that the higher C_p in this study is caused by measurement errors because of the small specimen size. This measurement error might be the reason of the sharp C_p increase at 1000°C.

Even though the Ti-Al-C sample in this study is actually composed of TI_2AlC, Ti_3AlC_2, and $Ti_5Al_2C_3$ phases, the C_p of these phases has been reported to be similar [16, 17] to each other. For this reason, the C_p is compared only with Ti_2AlC data in the literature [16], which was reported to be similar to those in this report in the temperature range of 25°C to 600°C. At temperatures above 600°C, a sharp increase in C_p is observed in our measurements while decrease in C_p was reported [16] and was attributed to the loss of aluminum atoms. The reason for sharp increase of C_p for Ti_2AlC at higher temperatures (> 800°C) is unclear, but might be related to the small sample size, which causes errors in the measurements. Another potential reason is the oxidation from residual oxygen in the Ar gas. The rather large data scattering for the three Ti-Si-C samples and the three Ti-Al-C samples used in this study also suggest large errors associated with the C_p measurements.

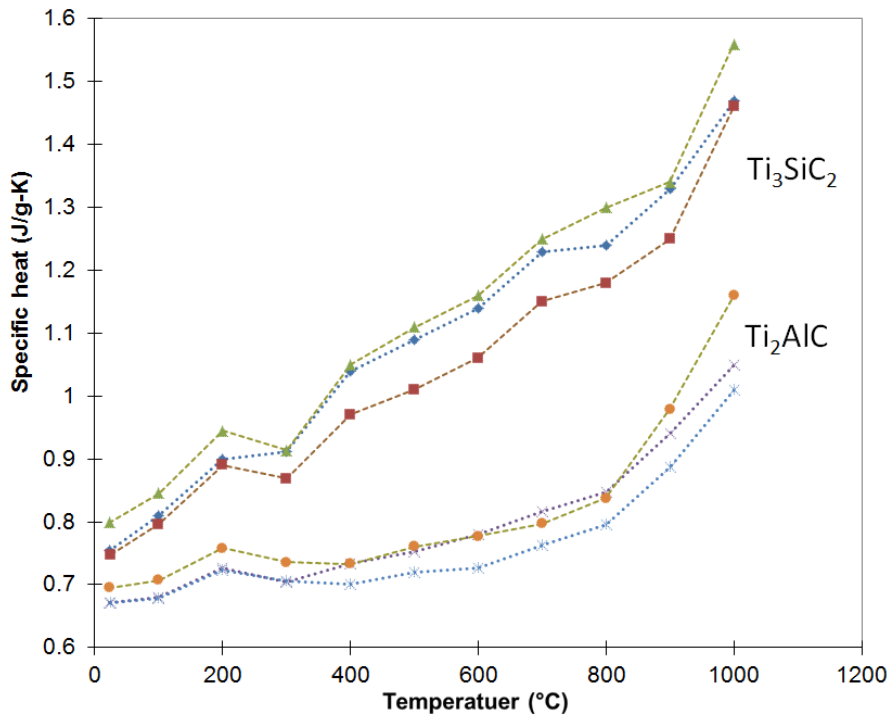

Figure 6. Measured specific heat of Ti-Si-C and Ti-Al-C (3 samples for each material).

The measured thermal diffusivity and calculated thermal conductivity are shown in Figure 7 and Figure 8, respectively. Ti-Si-C showed higher thermal diffusivity and conductivity than Ti-Al-C at all temperatures. Diffusivity of both materials decreases with increasing temperature.

Thermal diffusivity of relatively pure Ti_3SiC_2 has been reported to be ~15 mm^2/s at room temperature by two different research groups [14, 15], which is close to our measurement of ~14 mm^2/s, regardless of the higher fraction of impurity phases in this study. This indicates that the common impurity phases (mostly TiC) in the nominally Ti_3SiC_2 material has little effect in the overall thermal diffusivity of the material at non-irradiated state. The thermal conductivity is calculated from the product of measured density, measured Cp, and measured thermal diffusivity. The measured thermal conductivity of Ti-Si-C is higher than the values reported in the literature [9, 14] mainly because of higher measured C_p. The higher thermal conductivity and large increase of thermal conductivity at higher temperatures (above 800°C) is considered artifact caused by the measurement errors of C_p.

Thermal diffusivity and conductivity of Ti_2AlC has been reported by Barsoum *et al*. [12] and Bai *et al*. [18]. However, there is a large difference (46.0 W/m-K vs. 27.0 W/m-K at room temperature) between the two. In the former paper, the higher thermal conductivity is attributed to the phonon contribution, which is suggested to be much lower in the latter paper. The reason for the lower phonon thermal conductivity contribution in the Ti_2AlC in the latter paper is suggested to be related to the fine-grain microstructure and nonstoichiometry of the material, which both caused larger phonon scattering. In this report, the thermal diffusivity and conductivity are closer to the latter paper by Bei *et al*. [18]. Since the nominally Ti_2AlC in this study are mainly composed of other phases, a lower thermal conductivity can be expected.

Overall, both materials in this study have high thermal conductivities at non-irradiated states. However, neutron irradiation is known to reduce the thermal conductivity of materials. Hence the emphasis should be put on the thermal conductivities following neutron irradiation.

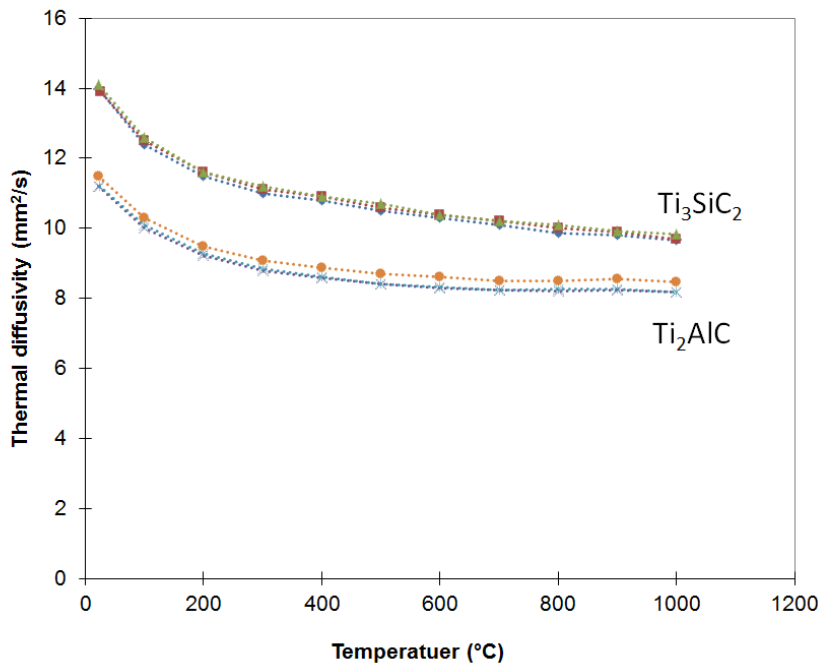

Figure 7. Measured thermal diffusivity of Ti_3SiC_2 and Ti_2AlC (3 samples for each material).

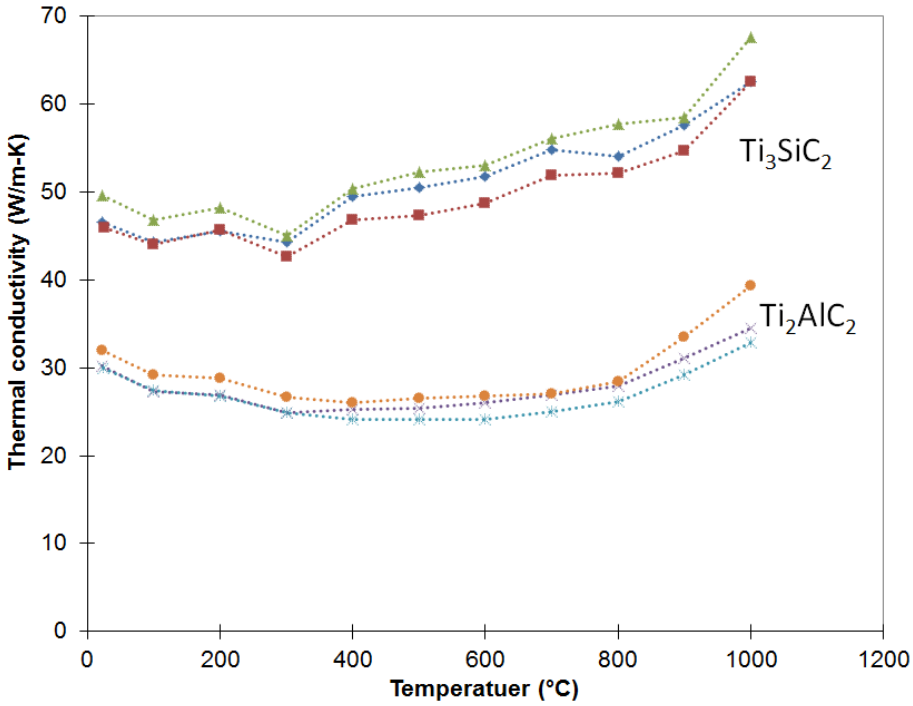

Figure 8. Calculated thermal conductivity of Ti_3SiC_2 and Ti_2AlC (3 samples for each material).

Dynamic Young's modulus

Average dynamic Young's moduli of Ti-Si-C and Ti-Al-C are listed in Table 1. At least 13 samples were measured for each material. Ti-Si-C showed an average Dynamic Young's modulus of 313 GPa with a coefficient of variation of 6.2%. This measured modulus is in line with the reported Young's modulus from the literature (322-333 GPa) [9]. It should be noted that TiC is an impurity in Ti_3SiC_2 that are difficult to eliminate because the structure similarity of TiC with Ti_3SiC_2. The amount of TiC in the nominally Ti_3SiC_2 material will affect the modulus.

Ti-Al-C showed a dynamic Young's modulus of 251 GPa with a coefficient of variation of 6.4%. The Young's moduli of Ti_2AlC and Ti_3AlC_2 have been summarized in reference [11] and are in the range of 267 to 306 GPa and 298 to 309 GPa, respectively. The Young's modulus for Ti-Al-C in this study appears to be slightly lower than the literature value.

Electrical resistivity

The average electrical resistivity of the nominally Ti-Si-C and Ti-Al-C are reported in Table 1. Ti-Si-C and Ti-Al-C have room temperature electrical resistivity of 0.285 and 0.467 mΩ-m, respectively. The coefficient of variation is in the range of 2 to 4%. Those materials are highly electrical conductive and have resistivity values comparable to some metals like iron, lead and titanium.

The electrical conductivity of Ti_3SiC_2 has been studied using *ab initio* calculations [19], which suggest that the conduction bands are provided almost entirely by the Ti 3d states. The measured electrical resistivity of 0.285 mΩ-m for Ti-Si-C is comparable with the literature values of 0.1 to 0.23 mΩ -m [9, 15]. The difference in the electrical conductivity can be attributed to the different microstructures and impurity phases of the materials used.

Theoretical work has shown that the high electrical conductivity of Ti_2AlC and Ti_3AlC_2 is related to the large $N(E_F)$, which is dominated by the Ti d-orbitals [11]. The electrical resistivity of Ti-Al-C in this study is consistent with the values reported in the literature for Ti_2AlC [18] and Ti_3AlC_2 [20].

Equibiaxial fracture strength and Weibull modulus

The average fracture strength and standard deviation of the two materials are listed in Table 1. The Weibull plots of Ti-Si-C and Ti-Al-C are shown in Fig. 9 and Fig. 10, respectively. Ti-Si-C showed a Weibull characteristic strength of 458 MPa with a weibull modulus of ~17. The average fracture strength of 445 MPa agrees well with the literature value of 450 MPa [9], indicating that the material is of good quality and that the equibiaxial fracture test with small specimens is a reliable and comparable test method.

The Weibull modulus of Ti_3SiC_2 from three-point bend fracture strength was reported to be 28.1 using the same statistical method [21]. The reason for the difference in modulus is unclear but is likely related to the different microstructure and different strength test methods.

Ti-Al-C showed a Weibull characteristic strength of 315 MPa with a weibull modulus of ~22. The average fracture strength value is close to the reported fracture strength of Ti_2AlC and Ti_3AlC_2 [11], which are in the range of 275 to 375 MPa.

When comparing the Weibull modulus of the two materials with monolithic SiC, which shows Weibull modulus between 2 and 12 [22], it is obvious that MAX phase materials have a much larger Weibull modulus, thus a better reliability performance, at the non-irradiated state.

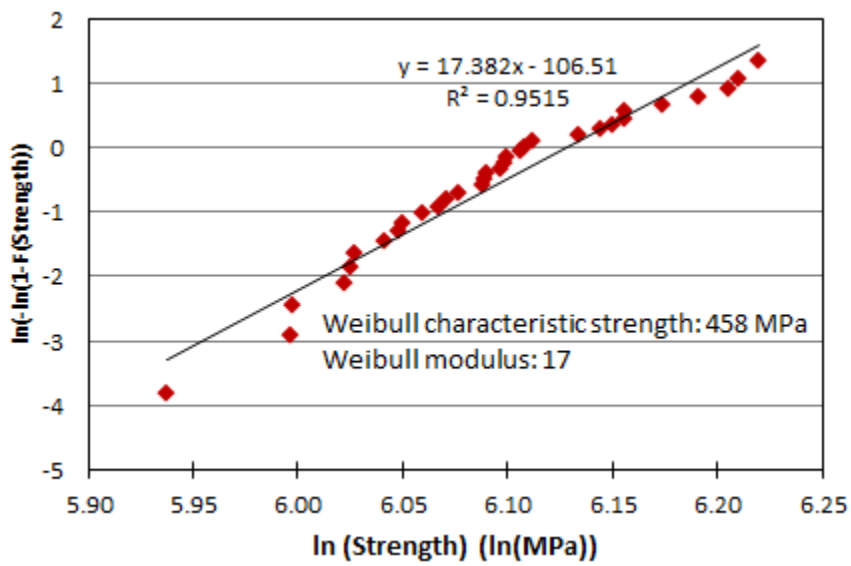

Figure 9. Weibull plot of Ti_3SiC_2.

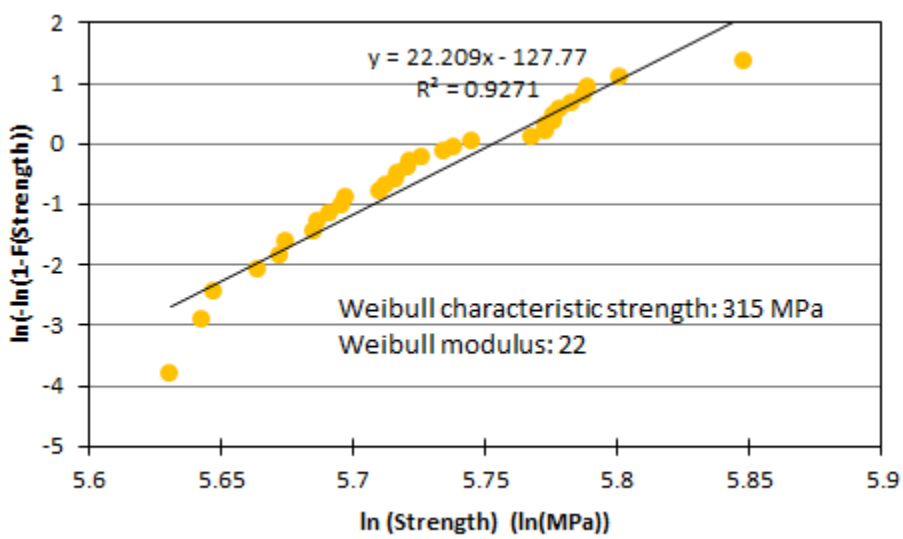

Figure 10. Weibull plot of Ti_2AlC.

CONCLUSIONS

This report summarized the physical and thermal mechanical properties of two commercially available MAX phase materials, normally Ti_3SiC_2 and Ti_2AlC, at non-irradiated states. The reported properties include: density, XRD analysis, microstructure analysis by SEM, CTE,

thermal diffusivity, thermal conductivity, dynamic Young's modulus, electrical conductivity, and equibiaxial fracture strength (including Weibull modulus). These properties are compared with existing data from the literature and good agreement is observed for all the properties studied.

The characterization of the non-irradiated MAX phase materials shows that these materials contain MAX phases of different stoichiometry and other non-MAX phase grains. The effect of radiation on the two materials likely will not represent that of pure phase materials. For this reason, the radiation effect will need to be examined carefully. However, techniques that characterize properties within one single grain would likely obtain representative information for a particular phase, assuming that phase and structure of the gain being studied is identified. Examples of such characterization techniques include transmission electron microscope analysis and nano-indentation.

REFERENCES

[1] N. J. Lane, S. C. Vogel, E. N. Caspi, and M. W. Barsoum, *J. Appl. Phys.* **113** (2013).
[2] M. W. Barsoum, *Prog. Solid State Chem.* **28** (2000) 201-281.
[3] E. N. Hoffman, D. W. Vinson, R. L. Sindelar, D. J. Tallman, G. Kohse, and M. W. Barsoum, *Nucl. Eng. Des.* **244** (2012) 17-24.
[4] X. M. Liu, M. Le Flem, J. L. Bechade, F. Onimus, T. Cozzika, and I. Monnet, *Nucl. Instrum. Methods Phys. Res. Sect. B-Beam Interact. Mater. Atoms* **268** (2010) 506-512.
[5] J. C. Nappé, P. Grosseau, F. Audubert, B. Guilhot, M. Beauvy, M. Benabdesselam, and I. Monnet, *J. Nucl. Mater.* **385** (2009) 304-307.
[6] J. C. Nappé, C. Maurice, P. Grosseau, F. Audubert, L. Thomé, B. Guilhot, M. Beauvy, and M. Benabdesselam, *J. Eur. Ceram. Soc.* **31** (2011) 1503-1511.
[7] J. C. Nappe, I. Monnet, F. Audubert, P. Grosseau, M. Beauvy, and M. Benabdesselam, *Nucl. Instrum. Methods Phys. Res. Sect. B-Beam Interact. Mater. Atoms* **270** (2012) 36-43.
[8] J. C. Nappe, I. Monnet, P. Grosseau, F. Audubert, B. Guilhot, M. Beauvy, M. Benabdesselam, and L. Thome, *J. Nucl. Mater.* **409** (2011) 53-61.
[9] H. B. Zhang, Y. W. Bao, and Y. C. Zhou, *J. Mater. Sci. Technol.* **25** (2009) 1-38.
[10] N. J. Lane, M. Naguib, J. Lu, L. Hultman, and M. W. Barsoum, *J. Eur. Ceram. Soc.* **32** (2012) 3485-3491.
[11] X. H. Wang and Y.C. Zhou, *J. Mater. Sci. Technol.* **26** (2010) 385-416.
[12] M. W. Barsoum, M. Ali, and T. El-Raghy, *Metall. Mater. Trans. A-Phys. Metall. Mater. Sci.* **31** (2000) 1857-1865.
[13] B. Manoun, F. X. Zhang, S. K. Saxena, T. El-Raghy, and M. W. Barsoum, *J. Phys. Chem. Solids* **67** (2006) 2091-2094.
[14] M. W. Barsoum, T. El-Raghy, C. J. Rawn, W. D. Porter, H. Wang, E. A. Payzant, and C. R. Hubbard, *J. Phys. Chem. Solids* **60** (1999) 429-439.
[15] Z. M. Sun, H. Hashimoto, Z. F. Zhang, S. L. Yang, and S. Tada, *Mater. Trans.* **47** (2006) 170-174.
[16] M. W. Barsoum, I. Salama, T. El-Raghy, J. Golczewski, W. D. Porter, H. Wang, H. J. Seifert, and F. Aldinger, *Metall. Mater. Trans. A-Phys. Metall. Mater. Sci.* **33** (2002) 2775-2779.
[17] A. Togo, L. Chaput, I. Tanaka, and G. Hug, *Phys. Rev. B* **81** (2010).
[18] Y. L. Bai, X. D. He, C. C. Zhu, and G. Q. Chen, *J. Am. Ceram. Soc.* **95** (2012) 358-364.
[19] Y. C. Zhou, Z. M. Sun, X. H. Wang, and S. Q. Chen, *J. Phys Condens. Matter* **13** (2001) 10001-10010.
[20] N. V. Tzenov and M. W. Barsoum, *J. Am. Ceram. Soc.* **83** (2000) 1551-1551.
[21] Y. W. Bao, Y. C. Zhou, and H. B. Zhang, *J. Mater. Sci.* **42** (2007) 4470-4475.

[22] L. L. Snead, T. Nozawa, Y. Katoh, T. S. Byun, S. Kondo, and D. A. Petti, *J. Nucl. Mater.* **371** (2007) 329-377.